Applied Catalysis B: Environmental 232 (2018) 314–321

Contents lists available at ScienceDirect

Applied Catalysis B: Environmental

journal homepage: www.elsevier.com/locate/apcatb

Enhancing fuel cell catalyst layer stability using a dual-function sulfonated silica-based ionomer

Reza Alipour Moghadam Esfahani, Holly M. Fruehwald, Foroughazam Afsahi, E. Bradley Easton*

Electrochemical Materials Lab, Faculty of Science, University of Ontario Institute of Technology, 2000 Simcoe Street North, Oshawa, Ontario, L1H 7K4, Canada

ARTICLE INFO

Keywords:
PEM fuel cell
Ceramic carbon electrode (CCE)
Sulfonated silica ionomer
Platinum electrocatalyst
Durability

ABSTRACT

Sulfonated-silica ceramic carbon electrodes (SS-CCE) were prepared by an *in-situ* sol-gel reaction where tetraethylorthosilicate and 3-trihydroxysilyl-1-propanesulfonic acid (TPS) are polymerized in the presence of a commercial Pt/C catalyst. The resultant catalyst layer is a promising candidate for application in proton exchange membrane fuel cells (PEMFCs), however their durability is unproven to date. To that end, we have examined the durability of these SS-CCE's in fuel cells. The SS-CCE was subjected to an accelerated stress testing (AST) and its fuel cell performance was assessed before and after the AST. Remarkably, the SS-CCE was substantially more durable than a conventional Nafion-based electrode employing the identical Pt/C catalyst. Detailed electrochemical tests and post-mortem analysis of each electrode revealed in addition to its primary function of conducting ions/retaining water, the sulfonated silica ionomer takes on the dual role of stabilizing the Pt/C catalysts through an electronic effect that mitigates Pt nanoparticles Ostwald ripening/agglomeration. The method for producing SS-CCE is highly versatile and could potentially be employed with any fuel cell catalyst. It is therefore proposed that this dual-function ionomer could be paired with almost any Pt/C (or supported alloy catalyst) and extend the operational lifetime of fuel cells without comprising beginning of life performance.

1. Introduction

Proton exchange membrane fuel cells (PEMFCs) have attracted the consideration of many researchers for clean portable power sources. Conventional catalyst layers are composed of platinum catalyst supported on carbon (Pt/C) with Nafion ionomer as a proton conductor [1–4]. However, there are serious concerns that these materials cannot withstand the harsh conditions under which fuel cells operate in the real world [5–7]. All three of these materials can chemical and/or mechanically degrade, which will in turn decrease performance. The carbon support is susceptible to corrosion in the cathode in which the electrode potential is relatively high in presence of oxygen species as follows:

$$C + 2H_2O \rightarrow CO_2 + 4H^+ + 4e^-,\ 0.207\,V\ vs\ NHE\ @\ 25\,^{\circ}C$$

Carbon corrosion leads to electrical isolation of Pt and a severe decline in the electronic conductivity of electrode [8–11]. Likewise, the degradation of Nafion ionomer performance can cause the ionic isolation of catalyst. Finally, Pt itself is prone is particle size growth via Ostwald ripening at high potentials in such an acidic environment.

One approach to alleviate these issues is to employ metal oxides as supporting materials. Metals oxides such as TiO_2, Ti_xO_{2x-1}, NbO_x, MoO_x and SiO_2 offer high catalytic activity and a strong interaction band with Pt NPs [12–22]. This can create a strong interfacial active band and enhance the catalytic activity towards the oxygen reduction reaction (ORR). Moreover, by employing oxide metals as a supporting material, a more stable and homogeneous dispersion of Pt particles can be achieved which also prevent the Pt NPs from agglomeration [23–27]. Ho et al. [28] developed a binary metal oxide support $Ti_{0.7}Ru_{0.3}O_2$ that acts as a co-catalyst supporting Pt in electroactivity, due to high proton conductivity of hydrated support. Jiang et al. [29] studied on Pt-Pd-Co electrocatalyst supported on titanium nitride nanorod arrays as the cathode of single cell without applying an ionomer. They claimed their developed electrocatalyst stand more stable than commercial gas diffusion electrode. While there is strong potential for metal oxides supports, many of these supports suffer from poor electronic conductivity [1], which limits their practical use in fuel cell devices.

Silicate-based materials have been investigated in fuel cell catalyst layers as a proton conducting alternative to Nafion. The catalyst layer structures are referred to as ceramic carbon electrodes (CCE), and have been shown have higher active surface area of Pt and good fuel cell performance [17,30,31]. Eastcott et al. [32] investigated sulfonated

* Corresponding author.
E-mail address: Brad.Easton@uoit.ca (E.B. Easton).

https://doi.org/10.1016/j.apcatb.2018.03.080
Received 17 October 2017; Received in revised form 13 March 2018; Accepted 22 March 2018
Available online 22 March 2018

silica-ceramic carbon electrodes (SS-CCE) in operating fuel cells and reported this electrode maintained stable performance with improved water management capabilities at low relative humidity, while Nafion-containing cathodes have performed poorly. Jung U.H. et al. [20] reported 40 wt.% addition of SiO_2 to the anode catalyst layer caused the current density at 0.6 V under 0% relative humidity achieve to 93% of that at 100% relative humidity. Wu Y.N. et al. [21] reported the addition of silicon oxide to Pt supporting martial enhanced the electrochemically active surface area and prevent the Pt NPs from agglomeration upon heating.

While these SS-CCE structures have the potential for lowering costs of fuel cell electrodes, their long-term durability in an operating PEM fuel cell is yet to be proven. In order to investigate this further, we have prepared SS-CCE's using a typical commercial electrocatalyst as well as a similar Nafion-based electrode using the same commercial electrocatalyst. Both electrodes were subjected to an accelerated stress testing (AST) that mimics a typical life time of operation in a fuel cell. Fuel cell performance was assessed before and after the AST for each and key electrochemical parameter were monitored throughout the tests. Our results have shown the sulfonated silica ionomer is stable throughout the tests. Furthermore, it was discovered that this ionomer serves a second function – the stabilization of the Pt, slowing its rate of agglomeration. This dual function enables the SS-CCE to outperform and outlast the conventional fuel cell electrode structure.

2. Experimental section

2.1. Chemicals

A commercial platinum catalyst 20 wt.% on carbon black Johnson Matthey, HiSPEC 3000 was purchased from Alfa Aesar. Gas diffusion layer (GDL) Elat LT1400W single sided was purchased from NuVant Systems Inc. 2-propanol (C_3H_8O) 99.5 wt.%, Methanol (CH_4O) 99.8 wt.%, Nafion® perfluorinated resin solution 5 wt.%, Ammonium hydroxide (NH_4OH) 28.0% NH_3 basis, tetraethylorthosilicate, 3-(trihydroxysilyl)-1-propanesulfonic acid (TPS, 30-35% in water) were purchased from Sigma Aldrich. Nafion® membrane was purchased from Ion Power, Hydrogen, Nitrogen and oxygen gases were supplied in cylinders by PRAXAIR with 99.999% purity. All aqueous solutions were prepared using ultrapure water obtained from a Millipore Milli-Q system with resistivity $>$ 18 mΩ cm.

2.2. Synthesis of electrodes

SS-CCE materials were prepared via the sol-gel method as outlined in our previous publications [32,33]. Briefly; 20% Pt on carbon black (HiSPEC3000) was mixed with deionized water and sonicated for 10 min, after which methanol and 6 M ammonium hydroxide were added to solution. The catalyst mixture was mechanically stirred for 1 hour, after which additions of tetraethylorthosilicate (TEOS) and 3-(trihydroxysilyl)-1-propanesulfonic acid (TPS, 30–35% in water) were added drop-wise to achieve a 5:95 TPS/TEOS mole ratio at a constant total silane concentration of ca. 40%. This mixture was stirred for 72 hours. The partially gelled Nafion-free SS-CCE was spray deposited onto the GDL and obtained electrodes were dried over vacuum plate at 50 °C for 2 hours, then transferred to oven at 110 °C for 1 hour. The SS-CCE had Pt loading of 0.22 mg cm^{-2}, tetraethylorthosilicate (TEOS) loading of 0.7 mg cm^{-2} and 3-trihydroxysilyl-1propanesulfonic acid (TPS) loading of 0.04 mg cm^{-2}. A Nafion-based electrode was also prepared through spray deposition method. The Pt/C electrode had Pt loading of 0.22 mg cm^{-2} and Nafion loading of 0.65 mg cm^{-2} (37.5 wt.%).

Membrane-electrode assemblies were fabricated by hot-pressing (150 kg cm^{-2} for 90 s at 110 °C) the two identical electrodes across a Nafion® 115 membrane (Ion Power Inc.) using a Carver laboratory press equipped with a temperature-controlled heating block. Nafion 115 was selected to minimize any effect of H_2 crossover in electrochemical diagnostic measurements MEAs were tested in a 5 cm^2 test fuel cell (Fuel Cell Technologies) on a commercial fuel cell test station (Fuel Cell Technologies) controlled using Labview software.

2.3. Physical characterization

XRD patterns were recorded on a Rigaku Ultima IV X-ray diffractometer that employs using Cu Kα radiation (λ = 0.15418 nm). Diffraction patterns were obtained over a 2θ range of 10–100° using a step size of 0.02°. Scanning Electron microscopy images and energy dispersive x-ray analysis were performed using a Hitachi FlexSEM 1000. Transmission electron microscopy (TEM) images of the Nafion-based Pt/C and Nafion-free SS-CCE electrocatalysts were acquired using a Zeiss Libra 200 MC Transmission Electron Microscopy (TEM) system operating at 200 kV. The TEM images were obtained by a technician at the University of Waterloo (WATLab).

2.4. Electrochemical characterization

The fuel cell performance were measured at the beginning of life and after the AST for MEAs prepared from each electrode. The fuel cell tests were performed at 80 °C with feed gases of (H_2 and O_2) pressurized to 1 bar at the outlets of both anode and cathode side. Gases were humidified by passing through humidifier bottles prior to entering the cell. Electrode durability was examined by exposing each MEA to an AST. During the AST, the cathode was exposed to nitrogen and the anode was exposed to hydrogen with flow rates of 200 and 100 ml min^{-1} respectively. The cell temperature was held constant at 25 °C, as was the anode and cathode humidifiers held constant at 25 °C. The AST consisted of 4000 potential cycles between 0.05 and 1.35 V vs RHE, with periodic assessment of electrode health by cyclic voltammetry (CV) and electrochemical impedance spectroscopy (EIS). CV measurements were used to determine the electrochemically active surface area (ECSA). EIS measurements were used to confirm the mode of degradation during the durability test. Impedance spectra were collected over a frequency range of 100 kHz–0.1 Hz at a DC bias potential of 0.425 V vs RHE [34,35]. All electrochemical measurements were performed by using a Solartron 1470E Multichannel potentiostat and paired with Solartron 1260 frequency response analyzer, controlled using Multistat software (Scribner Associates). Measurements were performed in triplicate for each MEA composition.

3. Results and discussion

3.1. Materials characterization

Fig. 1 shows TEM and SEM images obtained for the SS-CCE catalyst layer, including a layered EDS elemental distribution map. These images show the organosilicate in the SS-CCE is well dispersed, with a highly homogeneous distribution of silicon and Pt/C throughout. The TEM image of the SS-CCE shows that the Pt nanoparticles remain on the carbon surface and that the components are also homogeneously distributed at the nanoscale. Additional electron microscopy images including individual element maps can be found in Figure S1.

Fig. 2 compares the changes in the XRD patterns of each catalyst layer before and after the AST. For the Nafion-based catalyst later, the Bragg reflections expected for the face-centered cubic (fcc) structure of Pt were observed at 2θ values of 39.9° {111}, 46.3° {200}, 67.8° {220}, and 81.6° {311}. After the AST, the peaks became much sharper, indicating the growth in size of Pt particles. The Pt crystallite size was determined before and after the AST from the broadening of the {220} peak using the Scherrer equation. These values are listed in Table 1. For the Nafion-based electrode, the Pt crystallite size was found to increase from ca. 3.0 nm before the AST, to over 10 nm after the AST. This is consistent with the mode of degradation expected for this testing

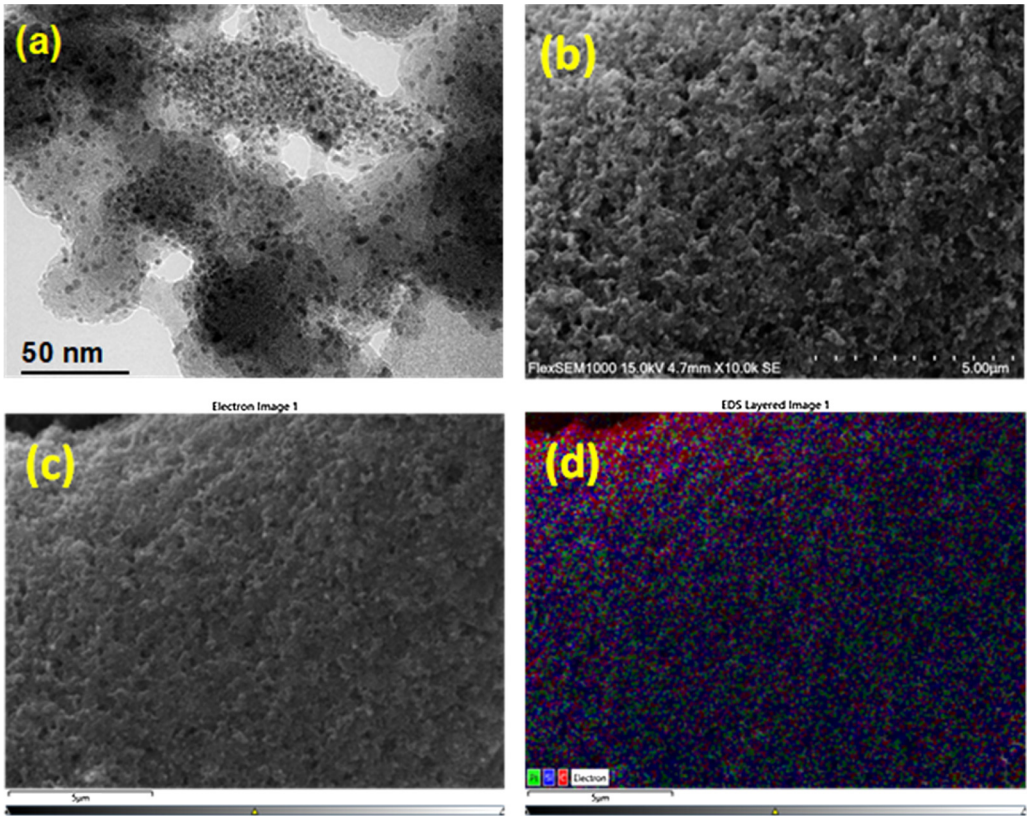

Fig. 1. (a) TEM image of the SS-CCE catalyst layer. (b) and (c) SEM image SS-CCE catalyst layer at different magnification. (d) EDX elemental mapping of SS-CCE catalyst layer overlayed onto the SEM image in (c).

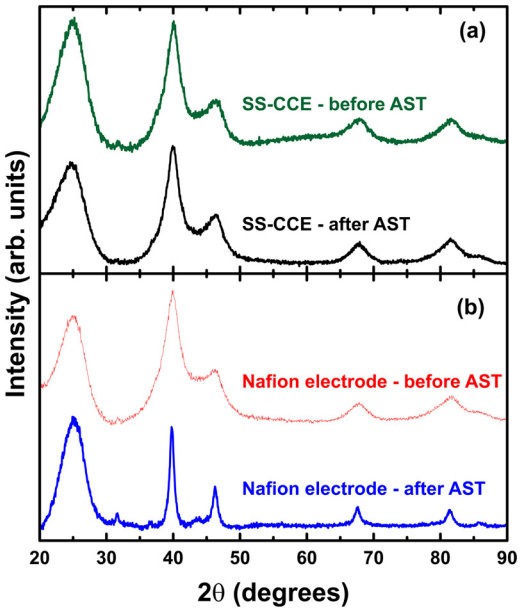

Fig. 2. XRD patterns obtained before and after the AST for the (a) SS-CCE and (b)Nafion- catalyst layers.

protocol [36]. The XRD pattern obtained for the SS-CCE catalyst layer contained the same peaks associated with fcc Pt, and the pattern changed very little after the AST. The Pt crystallite size before AST was determined to be 3.1 nm, and only grew to 3.4 nm after the AST. This signifies that the rate of Ostwald ripening was significantly slower in the SS-CCE compared to the Nafion-based catalyst layer.

Table 1
Summary of electrode properties.

	Nafion-based electrode	SS-CCE
Pt loading (mg/cm^2)	0.22	0.22
Pt grain size before AST (nm)	3.0	3.1
Pt grain size after AST (nm)	10.5	3.4
ECSA before AST (m^2/g$_{Pt}$)	57	74
ECSA after AST (m^2/g$_{Pt}$)	4	55
Peak power density before AST (mW/cm^2)	491	486
Peak power density after AST (mW/cm^2)	306	361

3.2. Electrochemical measurements

Fig. 3 compares the initial CVs obtained for the SS-CCE and Nafion-based catalyst layers. For both MEAs, the CVs exhibit three characteristic regions: the hydrogen adsorption and desorption region at low potential range, the double layer capacitance region between 0.35 and 0.50 V, and the Pt oxide formation and reduction region at high potentials. The SS-CCE displayed higher double layer capacitance compared to the Nafion-based electrode, though it did show more of a slope in the low potential region of the CV that is indicates it has a higher resistivity within the layer. The ECSA for each electrode was determined from the magnitude of the corresponding charge from the hydrogen underpotential (H_{UPD}) peaks (by applying a conversion factor of 210 µC cm^{-2}) after subtraction of the double layer background current. At the beginning of life, an ECSA value of 74 and 57 m^2 g^{-1} was obtained for SS-CCE and Nafion-based electrodes, respectively. The higher ECSA value obtained for SS-CCE is attributed to uniform distribution of the organosilicate, which resulted to greater proton accessibility to the Pt NPs active sites [21,37,38].

Apart from the high electrocatalytic activity, the durability of electrode is an important characteristic to identify the influence of

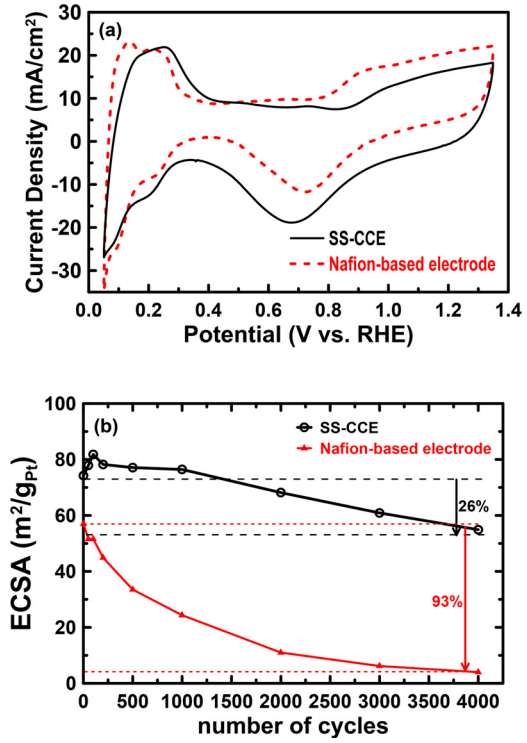

Fig. 3. (a) Comparison of the CVs obtained for the SS-CCE and Nafion-based Pt/C electrode at the beginning of fuel cell testing. (b) Variation in the ECSA of Pt with the number of potential cycles during the AST for each electrode.

electrochemical variation over potential cycling and its influence and contribution in loss of ECSA and consequently the electrodes activity [5,39,40]. In this study the durability test was conducted by subject each MEA to 4000 potential cycles. During the AST, CVs were collected periodically to measure ECSA. These CV collected for each electrode can be found in Figure S2. As the test progressed, there was a decline in the Pt features for each electrode. However, the decline in Pt surface features was much slower for the SS-CCE compared to the Nafion-based electrode. Fig. 3(b) plots the change in ECSA with potential cycle for each electrode. After 4000 cycles, the ECSA of SS-CCE declined by only 26%, while the Nafion-based electrode declined by 93% Table 1. This implies that the SS-CCE electrode is much more stable that the Nafion-based electrode. This is remarkable since both electrodes employed the same commercial catalyst from Johnson Matthey, meaning the catalysts used in both should inherently have the same durability. This implies that the organosilicate is stabilizing the electrode structure. To probe this mechanism further, the EIS data was examined since it can provide information about changes in conductivity and resistance in the catalyst layer under different conditions, as well as insight into degradation mechanisms [33,34,36]. Fig. 4 compares the initial EIS response for each electrode shown as Nyquist and capacitance plots. Both electrodes show good ionic conductivity, though the Nafion-base electrode exhibited a shorter Warburg length compared to the SS-CCE. This 45-degree Warburg region can be seen clearly in Fig. 4(b), which is an expansion of the high frequency region of the Nyquist plots. The projection of the Warburg length onto the real axis corresponds to a value of $R_\Sigma/3$, where R_Σ is the total catalyst layer resistance, which is the sum of ionic and electronic resistances in the catalyst layer. This data shows that the Nafion-based electrode has lower catalyst layer resistance than the SS-CCE. However, the SS-CCE has considerably higher capacitance, which could indicate greater accessible surface area of Pt/C. The EIS response of each electrode was monitored throughout the AST, and those plots are shown in Figure S3. For both electrodes, the EIS response changed subtly after the initial measurements, after which it was essentially unchanged. Analysis of the EIS was performed to extract both the membrane resistance (R_m) and R_Σ. The variation in R_m and R_Σ for each electrode is shown in Fig. 5. For each electrode, R_m and R_Σ decreased slightly during the early part of the AST, after which both they stabilized. This behavior is due to improved hydration in the catalyst layers over the course of testing [41]. With no increase in R_Σ during the course of the measurement, the modes of ionic and electronic conduction in the catalyst layer did not degrade in either electrode. The, along with the fact that the limiting capacitance was also

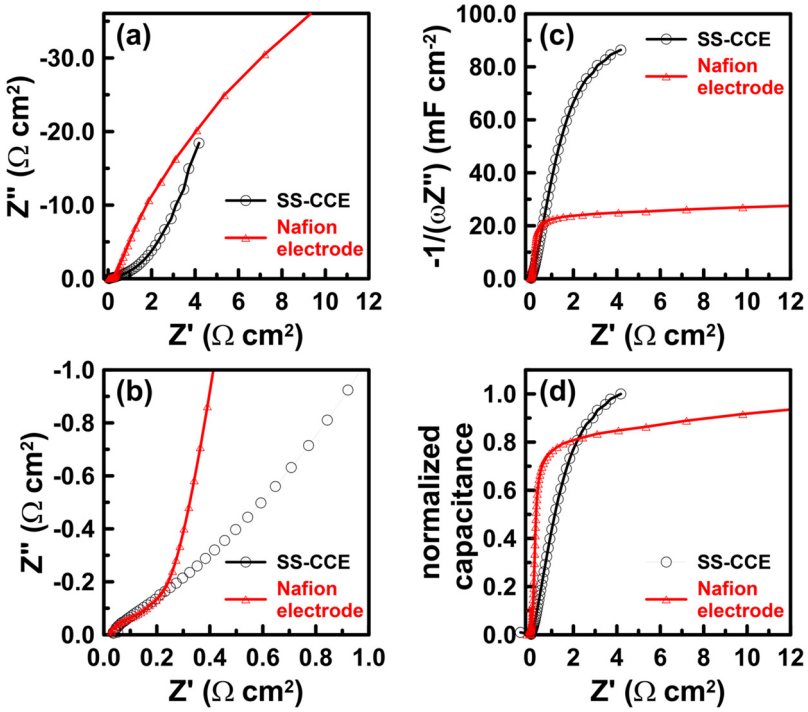

Fig. 4. Comparison of the EIS data obtained for the Nafion-based electrode and the SS-CCE at the beginning of testing. The data is displayed as (a) a Nyquist plot over the entire frequency range, (b) an expansion of the high frequency region of the Nyquist plot, (c) as a capacitance plot, and (d) as a nomalized capacitiance plot.

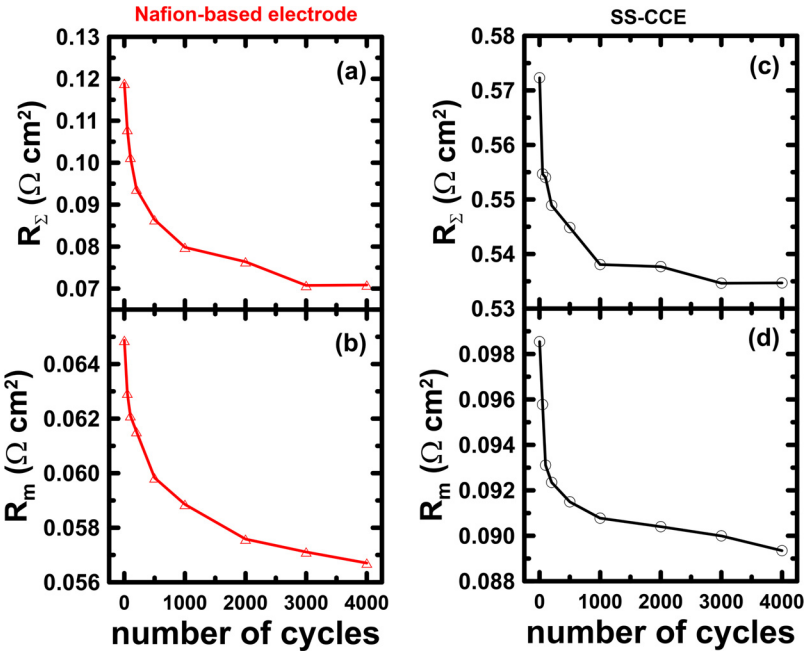

Fig. 5. The variation in (a) R_Σ and (b) R_m with number of potential cycles during the AST for the Nafion-based electrode. The variation in (c) R_Σ and (d) R_m with number of potential cycles during the AST for the SS-CCE.

stable for both, is indicative of a stable ionomer and a stable carbon support in both electrodes. This response profile is in fact the characteristic response when Pt particle size growth is the dominant degradation mechanism with the rate of Pt Ostwald ripening /agglomeration significantly faster in the Nafion-based electrode [36,41,42]. This is consistent with the XRD of the catalysts layers.

3.3. Fuel cell performance

Fig. 6 compares the fuel cell performance of each electrode before and after the AST. At the beginning of operation, both electrodes have almost the same performance, with the SS-CCE and Nafion-based electrodes yielding a maximum power density of 486 and 491 mW cm^{-2}, respectively. This is consistent with our previous report where we have shown that SS-CCE cathodes give performance on-par with conventional Nafion based cathodes [33,37]. After the AST, a decline in performance was observed for both electrode compositions. However, the decline in performance was more severe for the Nafion-based electrode compared to the SS-CCE. The peak power density achieved with the Nafion-based electrode declined to 306 mW cm^{-2} after the AST, a 38% decline compared to beginning of life. Given the fact that the ECSA decayed by over 90% during the AST, a larger decline in performance was expected for the Nafion-based electrode. Post mortem SEM analysis of the Nafion-based MEA is shown in Figures S4, which inidcated that there was considerable migration of Pt particles towards the membrane interface. The accumulate of Pt at this interface, where it is used most efficiently, may have partially mitigated the performance decline. It was also noteworthy that the Nafion-based elecotrde became thinner during the AST, going from 30 µm thick at the begining down to 18 µm after the AST.

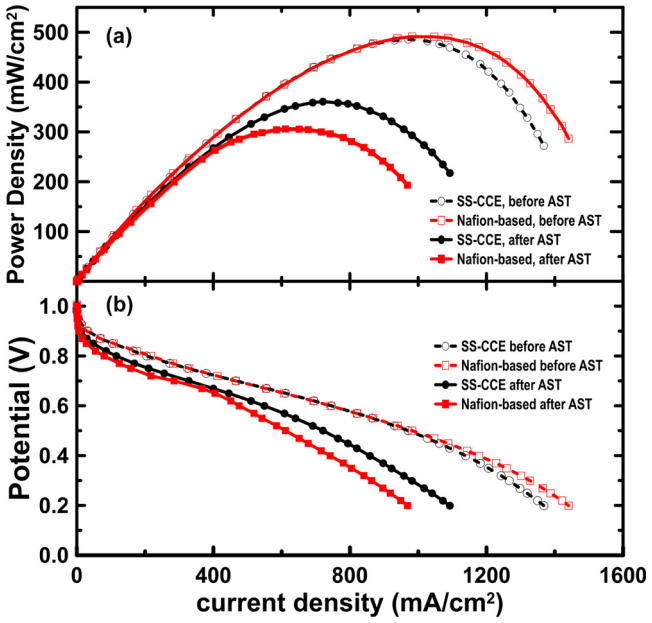

Fig. 6. Comparison of fuel cell performance before and after AST for the Nafion-based and SS-CCE electrode. Fuel cell testing was performed at 80 °C using humidified H_2 and O_2 gas feeds pressurized at the outlet to 1 bar. Performance is shown in (a) as power density vs. current density and in (b) as cell potential vs. current density.

The peak power density achieved with the SS-CCE declined to 361 mW cm^{-2}, a 25% decline compared to beginning of life. Fig. 7 compares cross-sectional SEM images obtained for the SS-CCE before and after the AST. The morphology and thickness of the SS-CCE catalyst layer remained stable over the course the AST. Furthermore, EDX mapping indicates there was essentially no change in the elemental distribution of the catalyst layer components before and after the AST. This indicates that the silicate structure remained stable and the large scale migration of Pt particles was mitigated in the SS-CCE. This demonstrates that the enhanced stability of the SS-CCE translates into better long-term performance in an operating fuel cell. Additional stability testing on the SS-CCE MEA can be found in the supplemental information.

It is clear from this work that the presence of the organosilicate ionomer enhances the stability of electrode. It does so by stabilizing the Pt in the electrode, slowing the rate of Pt particle size growth by Ostwald ripening. On the one hand, this is quite unexpected since one would not intuitively expect an ionomer to modify the stability of a catalyst. However, the organosilicate is not an ordinary catalyst layer

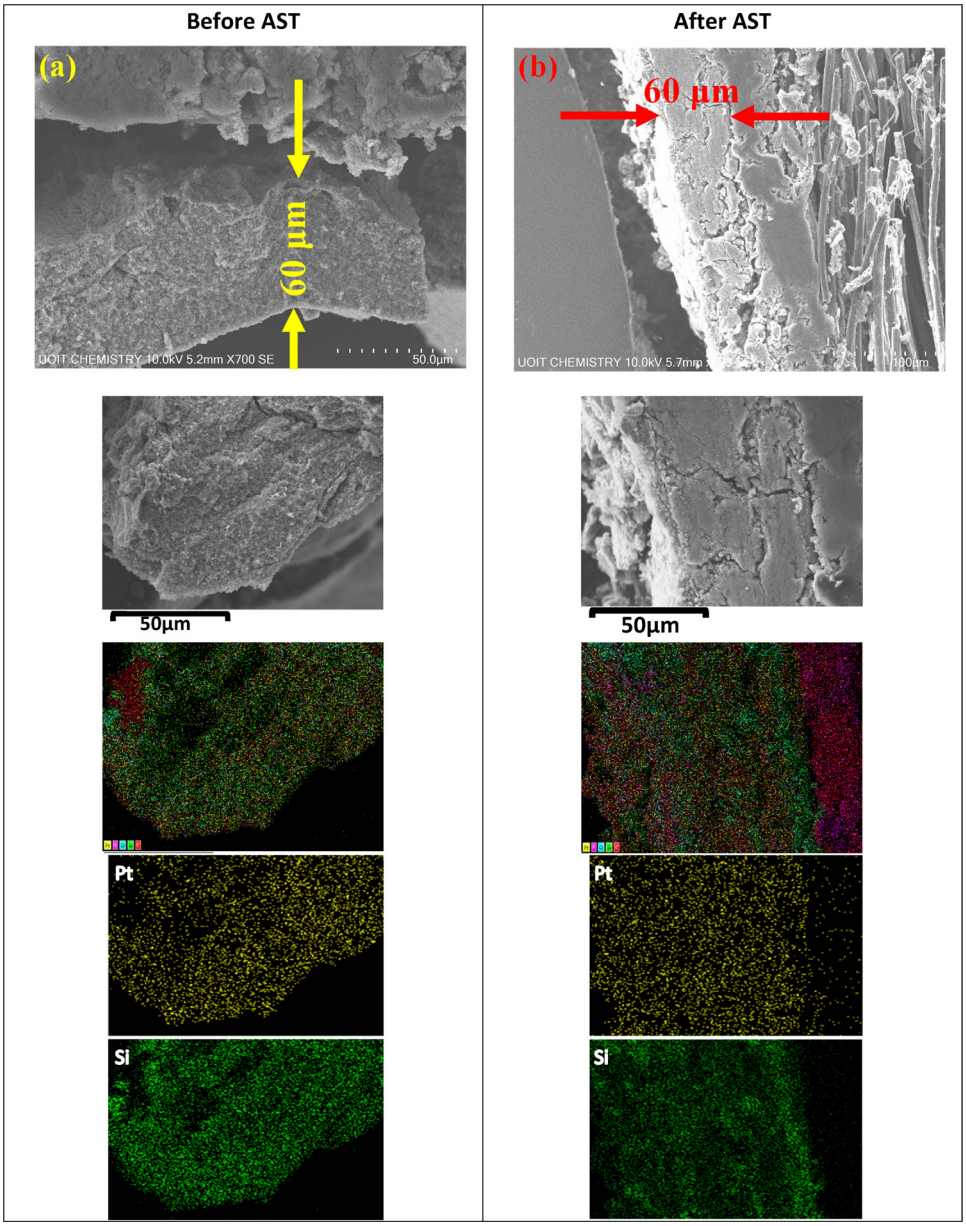

Fig. 7. Comparison of the cross-sectional SEM images and EDX elemental mapping obtained for the SS-CCE MEA (a) before, and (b) after the AST.

ionomer, which enables it to do more than simply aid in ion conduction. Because the organosilicate is formed by blending the Pt/C catalyst with the silane monomers, the ionomer network is able to grow around the dispersed Pt/C particles. This process not only leads to optimal distribution of the ionomer, but also to covalent bonding of the silicate to the carbon surface through surface −OH groups [43]. This brings the silicate network into intimate contact with the Pt surfaces, creating a strong electronic interaction with Pt nanoparticles greatly slows their rate of Ostwald ripening, agglomeration or migration into the bulk ionomer segment of the MEA [21,22,31,38,39]. A schematic depiction of the distribution is shown in Fig. 8. During CCE formation, the organosilane monomers create covalent bonds to the surface of the carbon support, also coming into intimate contact with the Pt surface. As the sol-gel reaction continues, the silicate network (shown in white) grows around the catalyst, and creates a porous network for longer range ion conduction and mass transport. This is not possible when employing conventional Nafion-based electrodes, where dispersed in Nafion is blended with the mechanically mixed with the catalyst. This top-down approach is not effective in creating a high degree of contact with the catalyst and leads to a high degree of agglomeration. It should be noted that Curnik and co-workers have reported that the addition of Nafion as an additive during the deposition of Pt nanoparticles can enhance the stability of the resultant Pt/C catalyst [44,45]. However, the extent of their durability testing was only a paltry 100 cycles, which is insufficient to draw any conclusion about Nafion's ability to enhance the long-term fuel cell stability of a Pt catalyst. The mode of stabilization in the SS-CCE is similar to that typically observed for metal oxide modified supports. However, unlike a metal oxide support, the SS-CCE provides a medium for ion and mass transport throughout the catalyst layer.

4. Conclusion

Nafion-free SS-CCE catalyst layers were synthesized through a one-step sol-gel method. Its fuel cell performance and durability was evaluated and compared to that of a conventional Nafion-based electrode employing the exact same Pt/C catalyst. Accelerated stress testing demonstrated the remarkable durability of the SS-CCE, whose ECSA loss was just 26% during the AST, compared to the 93% loss of the Nafion-

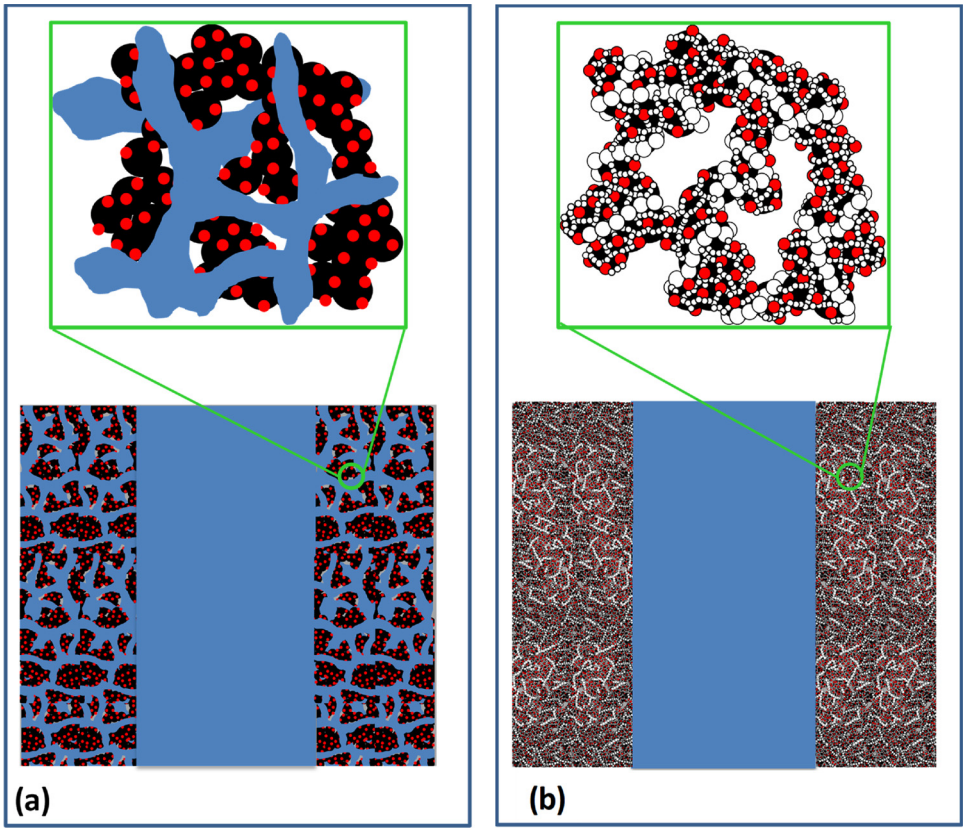

Fig. 8. The catalyst layer microstructure of (a) the conventional Nafion-based electrode and (b) the SS-CCE.

based Pt/C electrode. Fuel cell testing demonstrated equivalent performance was achieved for both electrodes at prior to the AST. However, after the AST, the decline in peak power performance was significantly larger for the Nafion-based electrode compared to the SS-CCE. Detailed electrochemical tests and post-mortem analysis of each electrode confirmed that Pt particle size growth and agglomeration was the reason for decline in both electrodes, and that the rate of growth/agglomeration was substantially lower for the SS-CCE. This enabled the SS-CCE to retain fuel cell performance better than the conventional Nafion-based electrode. The enhanced stability of the SS-CCE was attributed to the positive electronic effect of the co-functional sulfonated silica monomer that stabilizes the Pt nanoparticles from Ostwald ripening/agglomeration. In addition to its primary function of conducting ions/retaining water, the sulfonated silica ionomer takes on the dual role of stabilizing the Pt/C catalysts. The method for producing SS-CCE can be employed for any commercial or custom made carbon supported catalyst. It is therefore proposed that this dual-function ionomer could be paired with almost any Pt/C (or supported alloy catalyst) and extend the operational lifetime of fuel cells without comprising beginning of life performance.

Acknowledgements

This work was supported by the Natural Sciences and Engineering Research Council (NSERC) of Canada through the Strategic Grants program (Grant #STPGP 479094-15), Ballard Power Limited, and UOIT. The authors acknowledge equipment support from the Canada Foundation for Innovation. The authors thank Alan Young from Ballard Power for useful discussions. We also thank Dr. Joseph Jessy (University of Waterloo, WATLab) for acquiring the TEM images.

Appendix A. Supplementary data

Supplementary material related to this article can be found, in the online version, at doi:https://doi.org/10.1016/j.apcatb.2018.03.080.

References

[1] G.-F. Wei, Z.-P. Liu, Towards active and stable oxygen reduction cathodes: a density functional theory survey on Pt_2M skin alloys, Energy Environ. Sci. 4 (2011) 1268–1272.
[2] H.A. Gasteiger, S.S. Kocha, B. Sompalli, F.T. Wagner, Activity benchmarks and requirements for Pt Pt-alloy, and non-Pt oxygen reduction catalysts for PEMFCs, Appl. Catal. B Environ. 56 (2005) 9–35.
[3] W. Zhang, A.I. Minett, M. Gao, J. Zhao, J.M. Razal, G.G. Wallace, T. Romeo, J. Chen, Integrated high-efficiency Pt/carbon nanotube arrays for PEM fuel cells, Adv. Energy Mater. 1 (2011) 671–677.
[4] Z.Q. Tian, S.H. Lim, C.K. Poh, Z. Tang, Z. Xia, Z. Luon, P.K. Shen, D. Chua, Y.P. Feng, Z. Shen, J. Lin, Ahighly order-structured membrane electrode assembly with vertically carbon nanotunes for ultra-low Pt loading PEM fuel cells, Adv. Energy Mater. 1 (2011) 1205–1214.
[5] J. Wu, X.Z. Yuan, J.J. Martin, H. Wang, J. Zhang, J. Shen, S. Wu, W. Merida, A review of PEM fuel cell durability: degradation mechanisms and mitigation strategies, J. Power Sources 184 (2008) 104–119.
[6] D.P. Wilkinson, J. St-Pierre, W. Vielstich, H.A. Gasteiger, A. Lamm (Eds.), Handbook of Fuel Cells: Fundamentals, Technology and Applications, vol. 3, John Wiley & Sons Ltd., 2003, pp. 611–626.
[7] M.D. Gimenez-Lopez, A. Kurtoglu, D.A. Walsh, A.N. Khlobystov, Extremely stable platinum-amorphous carbon electrocatalyst within hollow graphitized carbon nanofibers for the oxygen reduction reaction, Adv. Mater. 28 (2016) 9103–9108.
[8] K. Sasaki, L. Zhang, R.R. Adzic, Niobium oxide-supported platinum ultra-low amount electrocatalysts for oxygen reduction, Phys. Chem. Chem. Phys. 10 (2008) 159–167.
[9] M. Cai, M.S. Ruthkosky, B. Merzougui, S. Swathirajan, M.P. Balogh, S.H. Oh, Investigation of thermal and electrochemical degradation of fuel cell catalysts, J. Power Sources 160 (2006) 977–986.
[10] A. Collier, H. Wang, X.Z. Yuan, J. Zhang, D.P. Wilkinson, Degradation of polymer electrolyte membranes, Int. J. Hydrogen Energy. 31 (2006) 1838–1854.
[11] D.-S. Kim, E.F. Abo Zeid, Y.-T. Kim, Additive treatment effect of TiO_2 as supports for Pt-based electrocatalysts on oxygen reduction reaction activity, Electrochim. Acta 55 (2010) 3628–3633.
[12] R. Alipour Moghadam Esfahani, A.H.A.Monteverde Videla, S. Vankova, S. Specchia,

Stable and methanol tolerant Pt/TiOx-C electrocatalysts for the oxygen reduction reaction, Inter. J. Hydrogen Energy 40 (2015) 14529–14539.
[13] C. Odetola, L.N. Trevani, E.B. Easton, Photo enhanced methanol electrooxidation: Further insights into Pt and TiO_2 nanoparticle contributions, Appl. Catal. B Environ. 210 (2017) 263–275.
[14] R. Alipour Moghadam Esfahani, S. Vankova, A.H.A.Monteverde Videla, S. Specchia, Innovative carbon-free low content Pt catalyst supported on Mo-doped titanium suboxide (Ti_3O_5-Mo) for stable and durable oxygen reduction reaction, Appl. Catal. B Environ. 201 (2017) 419–429.
[15] N.R. Elezovica, V.R. Radmilovic, N.V. Krstajic, Platinum nanocatalysts at metal oxide based supports for low temperature fuel cells applications, RSC Adv. 6 (2016) 6788–6801.
[16] Z. Zhang, J. Liu, J. Gu, L. Su, L. Cheng, An overview on metal oxide materials as electrocatalysts and supports for polymer electrolyte fuel cells, Energy Environ. Sci. 7 (2014) 2535–2558.
[17] R. Thangamuthu, C.W. Lin, Preparation of gas diffusion electrodes using PEG/SiO_2 hybrid materials and the effect of their composition on microstructure of the catalyst layer and on fuel cell performance, J. Power Sources 161 (2006) 160–167.
[18] K. Huang, Y. Li, L. Yan, Y. Xing, Nanoscale conductive niobium oxides made through low temperature phase transformation for electrocatalyst support, RSC Adv. 4 (2014) 9701–9708.
[19] J. Tang, H.M. Meng, TiO_2-modified CN_X nanowires as Pt electrocatalyst support with highly active and durable for oxygen reduction reaction, Phys. Chem. Chem. Phys. 18 (2016) 1500–1506.
[20] U.H. Jung, K.T. Park, E.H. Park, S.H. Kim, improvement of low-humidity performance of PEMFC by addition of hydrophilic SiO_2 particles to catalyst layer, J. Power Sources 159 (2006) 529–532.
[21] Y.-N. Wu, S.-J. Liao, J.-H. Zeng, Investigating the addition of silicon oxide to carbon: effects of amount and heat treatment on anti-aggregation and electrochemical performance of Pt catalysts, J. Power Sources 196 (2011) 1112–1117.
[22] Y. Zhang, J. Zang, L. Dong, X. Cheng, Y. Zhao, Y. Wang, A Ti-coated nano-SiC supported platinum electrocatalyst for improved activity and durability in direct methanol fuel cell, J. Mater. Chem. A 2 (2014) 10146–10153.
[23] P. Marques, N.F.P. Ribeiro, M. Schmal, D.A.G. Aranda, M.M.V.M. Souza, Selective CO oxidation in the presence of H_2 over Pt and Pt-Sn catalysts supported on niobia, J. Power Sources 158 (2006) 504–508.
[24] M. Tian, G. Wu, A. Chen, Unique electrochemical catalytic behavior of Pt nanoparticles deposited on TiO_2 Nanotubes, ACS Catal. 2 (2012) 425–432.
[25] S.-Y. Huang, P. Ganesan, B.N. Popov, Electrocatalytic activity and stability of titania-supported platinum palladium electrocatalysts for polymer electrolyte membrane fuel cell, J. Am. Chem. Soc. 2 (2012) 825–831.
[26] J. Greeley, J.K. Norskov, Combinatorial density functional theory-based screening of surface alloys for the oxygen reduction reaction, J. Phys. Chem. C. 113 (2009) 4932–4939.
[27] I. Chang, S. Ji, J. Park, M.H. Lee, W.S. Cha, Ultrathin YSZ coating on Pt cathode for high thermal stability and enhanced oxygen reduction reaction activity, Adv. Energy Mater. (2015), http://dx.doi.org/10.1002/aenm.201402251.
[28] V.T.T. Ho, K.C. Pillai, H.L. Chou, C.J. Pan, J. Rick, W.N. Su, B.J. Hwang, J.F. Lee, H.S. Sheu, W.T. Chuang, Robust non-carbon $T_{i0.7}Ru_{0.3}O_2$ support with co-catalytic functionality for Pt: enhancement catalytic activity and durability for fuel cell, Energy Environ. Sci. 4 (2011) 4194–4200.
[29] S. Jiang, B. Yi, H. Zhang, W. Song, Y. Bai, H. Yu, Z. Shao, Vertically aligned titanium nitride nanorod arrays as supports of platinum-palladium-cobalt catalysts for thin-film proton exchange membrane fuel cell electrodes, ChemElectroChem. 3 (2016) 734–740.
[30] L. Zheng, Q. Zeng, S. Liao, J. Zeng, Highly performed non-humidification membrane electrode assembly prepared with binary RuO_2-SiO_2 oxide supported Pt catalysts as anode, Int. J. Hydrogen Energy. 37 (2012) 13103–13109.
[31] S. Seok, I. Choi, K.G. Lee, B.G. Choi, K.J. Park, J.Y. Park, O.J. Kwon, S.J. Lee, D.H. Kim, Dopamine-induced Pt and N-doped carbon@silica hybrids as high-performance anode catalysts for polymer electrolyte membrane fuel cells, RCS Adv. 4 (2014) 42582–42584.
[32] J.I. Eastcott, E.B. Easton, Sulfonated silica-based fuel cell electrode structure for low humidity application, J. Power Sources 245 (2014) 487–494.
[33] J.I. Eastcott, J.A. Powell, A.J. Vreugdenhil, E.B. Easton, Electrochemical and morphological studies of ceramic carbon electrodes for fuel cell systems, ECS Trans. 41 (2011) 853–864.
[34] E.B. Easton, P.G. Pickup, An electrochemical impedance spectroscopy study of fuel cell electrodes, Electrochim. Acta 50 (2005) 2469–2474.
[35] O. Reid, F.S. Saleh, E.B. Easton, Determining electrochemically active surface area in PEM fuel cell electrodes with electrochemical impedance spectroscopy and its application to catalyst durability, Electrochim. Acta 114 (2013) 278–284.
[36] F.S. Saleh, E.B. Easton, Diagnosing degradation within PEM fuel cell catalyst layers using electrochemical impedance spectroscopy, J. Electrochem. Soc. 159 (2012) B546–B553.
[37] J.I. Eastcott, K.M. Yarrow, A.W. Pedersen, E.B. Easton, Fuel cell electrode structure containing sulfonated organosilane-based proton conductor, J. Power Sources 197 (2012) 102–106.
[38] J. Zeng, J. Chen, J.Y. Lee, Enhanced Pt utilization in electrocatalysts by covering of colloidal silica nanoparticles, J. Power Sources 184 (2008) 344–347.
[39] R.L. Borup, J.R. Davey, F.H. Garzon, PEM fuel cell electrocatalyst durability measurments, J. Power Sources 163 (2006) 76–81.
[40] W. Schmittinger, A. Vahidi, A review of the main parameters influencing long-term performance and durability of PEM fuel cells, J. Power Sources 180 (2008) 1–14.
[41] F.S. Saleh, E.B. Easton, Assessment of the ethanol oxidation activity and durability of Pt catalysts with or without a carbon support using electrochemical impedance spectroscopy, J. Power Sources 246 (2014) 392–401.
[42] O. Reid, F.S. Saleh, E.B. Easton, Application of the transmission line EIS model to fuel cell catalyst layer durability, ECS Trans. 61 (2014) 25–32.
[43] E.B. Easton, Z.G. Qi, A. Kaufman, P.G. Pickup, Chemical modification of proton exchange membrane fuel cell catalysts with A sulfonated silane, Electrochem. Solid-State Lett. 4 (2001) A59–A61.
[44] O.J. Curnick, B.G. Pollet, P.M. Mendes, Nafion@-stabilised Pt/C electrocatalysts with efficient catalyst layer ionomer distribution for proton exchange membrane fuel cells, RSC Adv. 2 (2012) 8368–8374.
[45] O.J. Curnick, B.G. Pollet, P.M. Mendes, Enhanced durability of a Pt/C electrocatalyst derived from nafion-stabilised colloidal platinum nanoparticles, Electrochem. Commun. 12 (2010) 1017–1020.